ORIGINAL RESEARCH

Open Access

Imaging Aβ and tau in early stage Alzheimer's disease with [18F]AV45 and [18F]AV1451

Azadeh Firouzian[1*] (iD), Alex Whittington[2], Graham E. Searle[1], Ivan Koychev[3], Giovanna Zamboni[4], Simon Lovestone[3], and Roger N. Gunn[1,2,5] on behalf of the Deep and Frequent Phenotyping study team

Abstract

Background: AD is a progressive neurodegenerative disorder that is associated with the accumulation of two different insoluble protein aggregates, Aβ plaques and hyperphosphorylated tau. This study aimed to investigate the optimal acquisition and quantification of [18F]AV45 and [18F]AV1451 to image Aβ and tau, respectively, in subjects with AD.

Fifteen subjects with early stage AD underwent a T1-weighted structural MRI and two dynamic PET scans to image Aβ (60 min, [18F]AV45) and tau (120 min, [18F]AV1451). Both dynamic BP_{ND} and static SUVR outcome measures were calculated and compared for 12 out of 15 subjects who completed 60 min of the Aβ PET scan and at least 110 min of the tau PET scan. The SRTM and reference Logan graphical analysis were applied to the dynamic data to estimate regional BP_{ND} values and SUVR ratios from the static data. Optimal acquisition windows were explored for both the dynamic and static acquisitions. In addition, the spatial correlation between regional Aβ and tau signals was explored.

Results: Both the SRTM and graphical analysis methods showed a good fit to the dynamic data for both Aβ and tau dynamic PET scans. Mean regional BP_{ND} estimates became stable 30 min p.i. for [18F]AV45 and 80 min p.i. for [18F]AV1451.

Time stability analysis of static SUVR data showed that the outcome measure starts to become stable for scan windows of 30–50 min p.i. for [18F]AV45 and 80–100 min p.i. for [18F]AV1451. The results from these time windows correlated well with the results from the full dynamic analysis for both tracers ($R^2 = 0.74$ for [18F]AV45 and $R^2 = 0.88$ for [18F]AV1451). There was a high correlation between amyloid uptake estimate using both dynamic analysis methods in thalamus and tau uptake in thalamus, hippocampus and amygdala.

Conclusions: Short static PET scans at appropriate time windows provided SUVR values which were in reasonable agreement with BP_{ND} values calculated from dynamic scans using SRTM and reference Logan. These simplified methods may be appropriate for classification and intervention studies, although caution should be employed when considering interventional studies where blood flow and extraction could change.

Keywords: Alzheimer's disease, PET, Amyloid, Tau, Modelling

---

* Correspondence: Azadeh.Firouzian@imanova.co.uk
[1]Imanova Ltd., Burlington Danes Building, Imperial College London, Hammersmith Hospital, Du Cane Road, London W12 0NN, UK
Full list of author information is available at the end of the article

Firouzian *et al. EJNMMI Research* (2018) 8:19

Page 2 of 9

Background

Alzheimer's disease (AD) is a progressive neurodegenerative disorder that is associated with the accumulation of two different insoluble protein aggregates, amyloid-β (Aβ) plaques and neurofibrillary tangles (NFTs) consisting of hyperphosphorylated tau protein. Evidence suggests that both Aβ and NFTs have known involvement in AD together with other less explored contributors [1]. The pathophysiological process of AD begins years before the clinical symptoms appear [2–4] and this preclinical phase provides an opportunity for therapeutic intervention. Molecular imaging of Aβ and tau could provide important tools for stratifying subjects in this preclinical phase and assessing the impact of novel drug therapies [5, 6].

Positron emission tomography (PET) radioligands are now available to image both insoluble Aβ plaques and tau neurofibrillary tangles relevant for AD [7]. Aβ imaging has been feasible since 2004 [8] following the introduction of [^{11}C]PiB and a number of fluorinated Aβ radiotracers (Florbetapir ([^{18}F]AV45), [^{18}F]Florbetaben, [^{18}F]Flutemetamol) that have been approved by European medicines agency (EMA) as well as food and drug agency (FDA). These tracers are being used in clinical trials for stratification and to assess Aβ levels pre and post therapy [6, 9]. More recently, efforts have focused on developing tracers suitable for imaging tau [10].

Initial studies have demonstrated that there are radiotracers that bind to tau and provide signals that are consistent with postmortem data [11–13]. One of the first generation tau tracers that has demonstrated such signals is [^{18}F]AV1451 ([^{18}F]T807) with evident in vivo differences between healthy controls and AD subjects that generally reflect the expected spatial distribution of tau in AD [14].

The data presented here, involving [^{18}F]AV45 and [^{18}F]AV1451, were acquired as part of the pilot phase of the UK medical research council-sponsored (MRC) deep and frequent phenotyping study which aims to identify stratification markers and markers of change in the preclinical phase of AD subjects. The pilot phase aimed to determine participants' acceptability of extensive and repeated phenotyping, the practicality of this procedure and to establish an optimal protocol for the main study.

This paper aims to assess the PET imaging data acquired as part of the pilot study, including dynamic Aβ and tau scans, to provide better understanding of the data and working towards designing an efficient protocol for the main study. Different acquisition (dynamic vs static) and analysis procedures will impact on the outcome measures derived and were investigated with this data set. Full kinetic analysis of the dynamic PET scans was performed using quantitative reference tissue approaches including the simplified reference tissue model

(SRTM) [15, 16] and reference Logan graphical analysis [17] to derive the non-displaceable binding potential (BP$_{ND}$). Additionally, the simpler static measure of standardized uptake value ratio (SUVR) was obtained from these data at various time windows and compared against the full dynamic quantification to assess outcome measure stability and bias. Finally, the spatial relationship between Aβ and tau was investigated across the subjects that had been scanned.

Methods

Subjects

Fifteen subjects were included in the analysis, with a diagnosis of mild AD (with no AD pathophysiological evidence) according to national institute of aging-Alzheimer's association (NIA-AA) criteria [18–21], aged between 54 and 83 years, with a mini mental state examination (MMSE) score of 21–29 and a modified Hachinski ischemic score (HIS) of less than 4 [22]. All subjects underwent a series of assessments including clinical, cognitive, gait and ophthalmological assessments, as well as molecular markers in cerebrospinal fluid (CSF), blood, urine, PET imaging, magnetic resonance imaging (MRI), magnetoencephalography (MEG) and electroencephalography (EEG). The study was approved by the institutional review board and all subjects signed an informed consent form (ICF).

Image acquisition

All subjects underwent a 3D T1-weighted structural MRI and two dynamic PET scans to image Aβ and tau on separate days. Acquisitions were conducted in accordance with the international conference on harmonisation (ICH) guideline for good clinical practice (GCP) and the ethical principles that have their origins in the declaration of Helsinki. The institutional review board/ethics committee reviewed and approved the protocol and ICFs as well as any advertising and subject materials before any subjects were enrolled. A written, signed and dated ICF was provided before any protocol was performed.

The MRI scan was performed on a Siemens 3T Tim Trio with a 32-channel phased array head coil. A 1 mm isotropic whole-brain structural 3D T1-weighted MPRAGE [23] was acquired using TI = 880 ms, TR = 2000 ms and FA = 8° with a parallel imaging factor of 2 in 4 m: 54 s. For the PET scans, subjects were positioned in the PET scanner after the insertion of a venous cannula in an antecubital or forearm vein, and a head-fixation device was used to minimize head movement during data acquisition. The PET scans were acquired on two Siemens PET/CT (computed tomography) scanners (Hi-Rez Biograph 6 and Biograph 6 TruePoint with TrueV, Siemens Healthcare, Erlangen, Germany), though for consistency each subject had both of their PET scans on the same scanner.

Firouzian *et al. EJNMMI Research* (2018) 8:19

Page 3 of 9

A low-dose CT scan was performed immediately before each PET scan in order to estimate attenuation. Each subject received a single intravenous bolus of [¹⁸F]AV45 (150 ± 24 MBq) for a 60 min Aβ PET scan and [¹⁸F]AV1451 (163 ± 10 MBq) for a 120 min tau scan. The dynamic images were reconstructed using a 2D filtered back projection (FBP) algorithm resulting in a 128 × 128 matrix with 2 mm isotropic voxels. Corrections were applied for attenuation, randoms, scatter and radioactive decay.

Image analysis

Two different classes of image analysis approaches were investigated in this study: static and dynamic. In both approaches, the T1-weighted MRI scan was used to obtain anatomical information for each subject. Each subject's whole brain was extracted using the Oxford centre for functional MRI of the brain (FMRIB) software library (FSL) [24] brain extraction tool (BET) [25] and the corresponding grey matter probability maps were created using statistical parametric mapping (SPM5) software [26]. A template MRI (ICBM152 [27]) was then nonlinearly warped to subject's MRI using SPM5 and the resulting deformation was applied to a brain anatomical atlas [28] consisting of 119 brain regions to obtain the brain region boundaries for each subject. This individualized atlas was used at a later stage to derive regional tissue time activity data from the dynamic PET images.

The dynamic PET images (2 × 2 × 2 mm) were initially motion corrected by rigidly registering each frame to a reference frame (13–15 min p.i.) using mutual information and subsequently rigidly transformed into alignment with the MRI and individualized atlas. The chosen reference frame contains both information on delivery and uptake allowing for both early and late frames to be aligned effectively. Finally, to be able to calculate different parameters, the atlas in the individualized Montreal neurological institute (MNI) space is down-sampled to match PET voxel size.

Regional time activity curves (TACs) were generated using the atlas and dynamic PET images. The SRTM and reference Logan graphical analysis with cerebellum grey matter as reference region were applied to the regional TACs to estimate the BP_{ND}, used to quantify the amount of tracer binding to the target proteins. Parametric images for both measures were also created by applying the models to each voxel [16].

The SRTM model equation is given by,

$$C_T(t) = R_1 C_R(t) + \left(k_2 - \frac{R_1 k_2}{1 + BP_{ND}} \right) C_R(t) \otimes e^{-\frac{k_2}{(1+BP_{ND})} t}$$

(1)

where $C_T(t)$ is the activity concentration in the target tissue, $C_R(t)$ is the activity in reference tissue, k_2 is the

efflux rate constant from target tissue, R_1 is the ratio of the delivery in target region to reference region. R_1, k_2 and BP_{ND} are estimated for each region.

The reference Logan graphical analysis method is given by,

$$\frac{\int_0^t C_T(s)ds}{C_T(t)} = (1 + BP_{ND}) \frac{\int_0^t C_R(s)ds}{C_T(t)} + \text{int} \quad \text{for } t > t*$$

(2)

where BP_{ND} is the binding potential, 'int' is the regression intercept and t^* is the equilibrium time.

The distribution of estimated regional BP_{ND} values using the two reference tissue analysis methods from tau and Aβ PET scans over all subjects was compared to assess the performance of each method.

For the static analysis, SUVR values (Eq. 3) were calculated using cerebellum grey matter as the reference region. Regional average SUVR values were calculated for 20 min time windows for a range of different start times post injection (p.i.) (between 0 and 60 min for [¹⁸F]AV45 and between 0 and 120 for [¹⁸F]AV1451) from static images created by averaging the frames in each time window.

$$SUVR(t) = \frac{SUV_{Target}(t)}{SUV_{Reference}(t)}$$

(3)

where SUV_{Target} is the SUV of the target region and $SUV_{Reference}$ is the SUV of the reference region.

Additionally, the time stability of both dynamic (BP_{ND}) and static (SUVR) outcome measures and their relationship were investigated. The BP_{ND} values were calculated for several scan durations by reducing the scan duration with steps of 10 min and the SUVR values were calculated for 20 min time windows created by splitting the scan period into 20 min time windows. The relation between these two measures was assessed by performing a regression analysis. Additionally, the correlation between regional Aβ and tau signals was explored.

All the above mentioned analysis was performed using molecular imaging and kinetic analysis toolbox (MIA-KAT™, version 4.0.2, http://www.miakat.org/MIAKAT2/index.html).

Results

All subjects successfully completed the 60 min Aβ PET scans and 12 out of 15 completed at least 110 min of the tau PET scan—these 12 subjects were included in the analysis that is presented here. The included subjects had an average age of 71.4 ± 10.1, modified HIS score of 0.8 ± 1.0, mild cognitive impairment with MMSE score of 24.3 ± 2.1 and Alzheimer's disease assessment scale-cognitive (ADAS-Cog) score of 15.5 ± 7.1. Mean symptom duration was 3.5 ± 2.1 years and mean time since

Firouzian *et al. EJNMMI Research* (2018) 8:19

Page 4 of 9

the initial diagnosis was 1.3 ± 2.1 years which was confirmed as an inclusion criteria at the time of the PET scan.

Dynamic analysis

TACs and SRTM (Eq. 1) kinetic fits were successfully generated for all 119 atlas regions of interest (ROIs) for both Aβ and tau dynamic PET scans for all subjects. The SRTM with cerebellum grey as reference region was fitted to the TACs for each region (Fig. 1a, b) and the three parameters (R_1, k_2 and BP_{ND}) were estimated per region. The TACs show that the tau signal from [^{18}F]AV1451 has slower kinetics and less regional distinction in comparison to the Aβ signal from [^{18}F]AV45. Similarly, reference Logan graphical analysis (Eq. 2) with cerebellum grey as reference tissue was fitted to the TACs (Fig. 1c, d) and the two parameters (BP_{ND} and int) were estimated per atlas region for each subject. Both models showed a good fit to the data for both Aβ and tau dynamic PET scans.

To investigate the approximate time at which regional BP_{ND} values stabilize, the mean regional BP_{ND} values derived using SRTM averaged over all subjects was plotted against scan duration for both Aβ and tau dynamic PET scans (Fig. 2a, b). Mean regional BP_{ND} estimates become stable after 30 min p.i. for [^{18}F]AV45 and after 80 min p.i. for [^{18}F]AV1451 for all regions. Similar analysis was performed to the same PET scans using reference Logan graphical analysis model with cerebellum grey as reference region and mean regional BP_{ND} values were estimated for all subjects using a range of starting time points (t^*) for the regression analysis (Fig. 2c, d). For t^* values of over 30 min, the BP_{ND} values are stable for Aβ scans, whereas stability occurs at t^* greater than 70 min for tau. The estimated regional BP_{ND} values using the two dynamic models were compared over all subjects for Aβ and tau dynamic PET scans (Fig. 3). Similar regional BP_{ND} values were estimated by both dynamic models but overall, the regional BP_{ND} values estimated by SRTM were higher on average with larger variation across subjects.

Static analysis

The static analysis involved the calculation of regional SUVR values for 20 min scan windows spanning the full scan duration using Eq. 3 with the grey matter cerebellum as the reference region. The time stability of mean regional SUVR was assessed for several regions for all subjects (Fig. 4) for Aβ and tau PET scans which showed that the
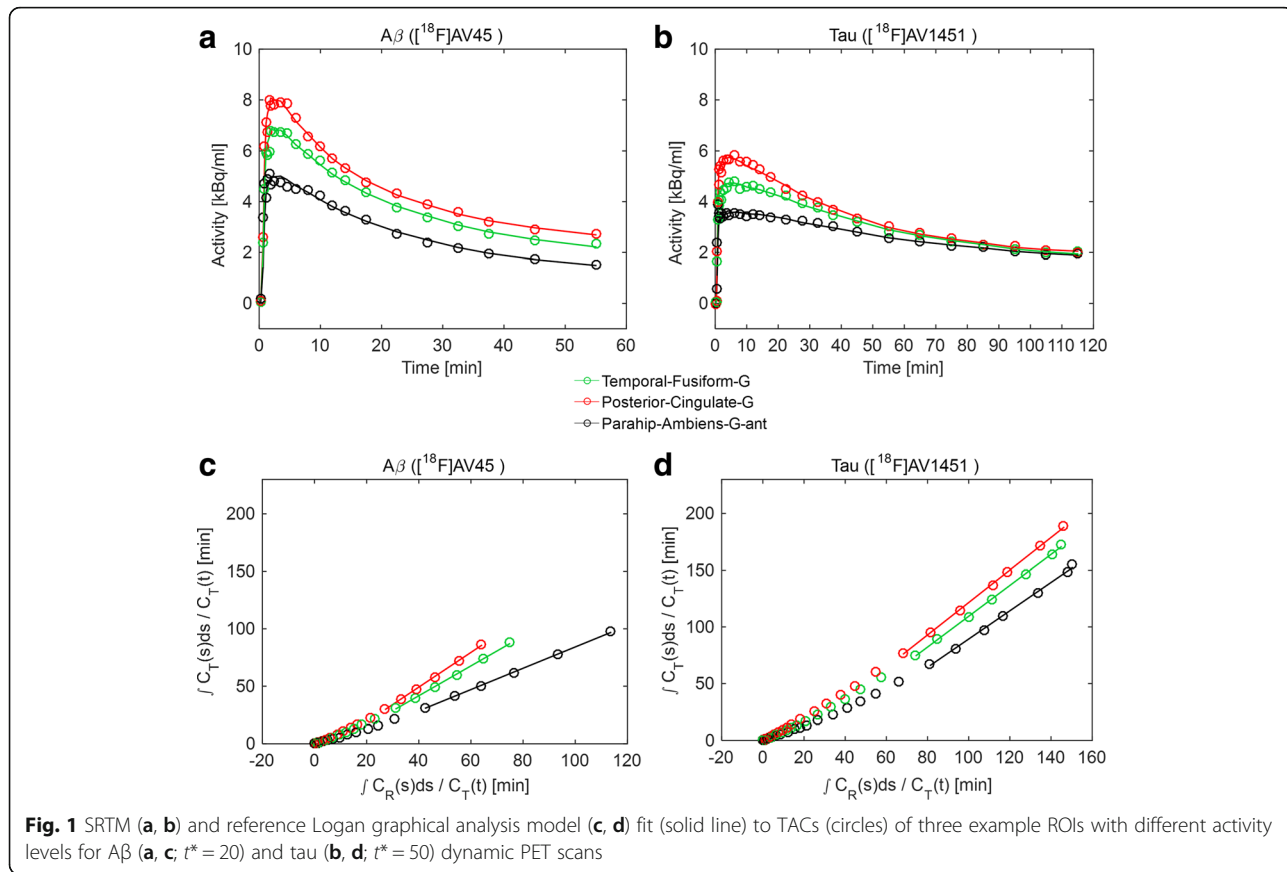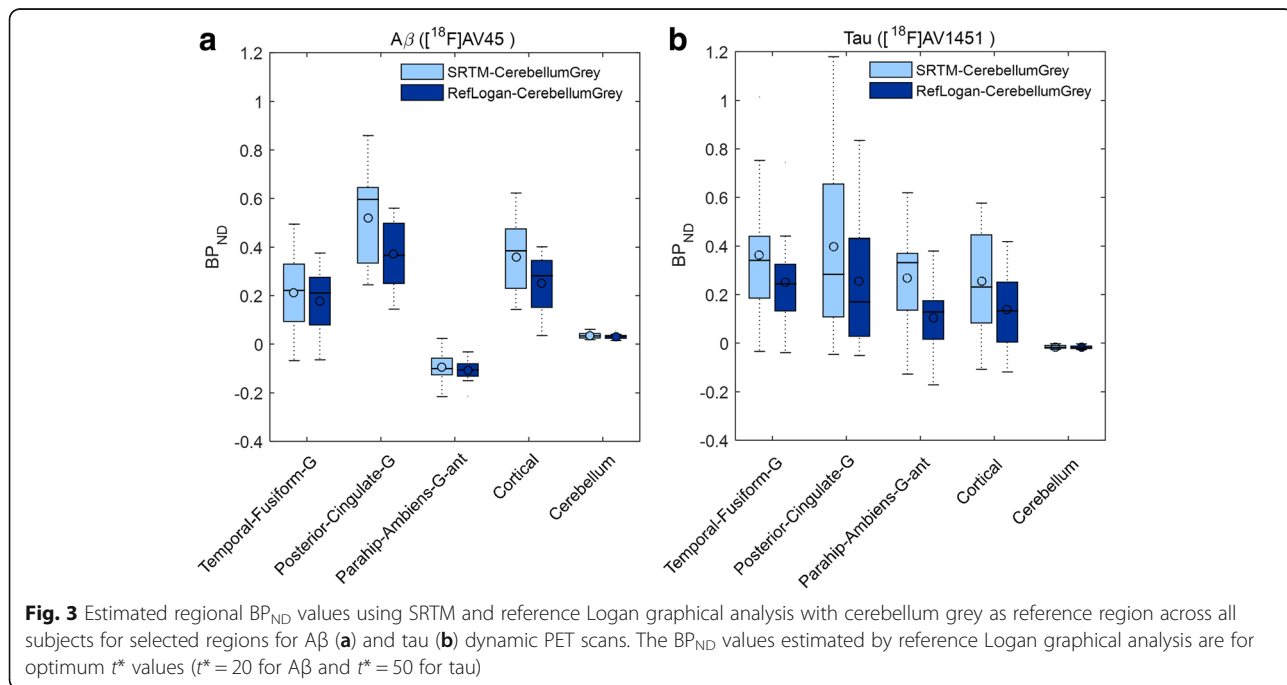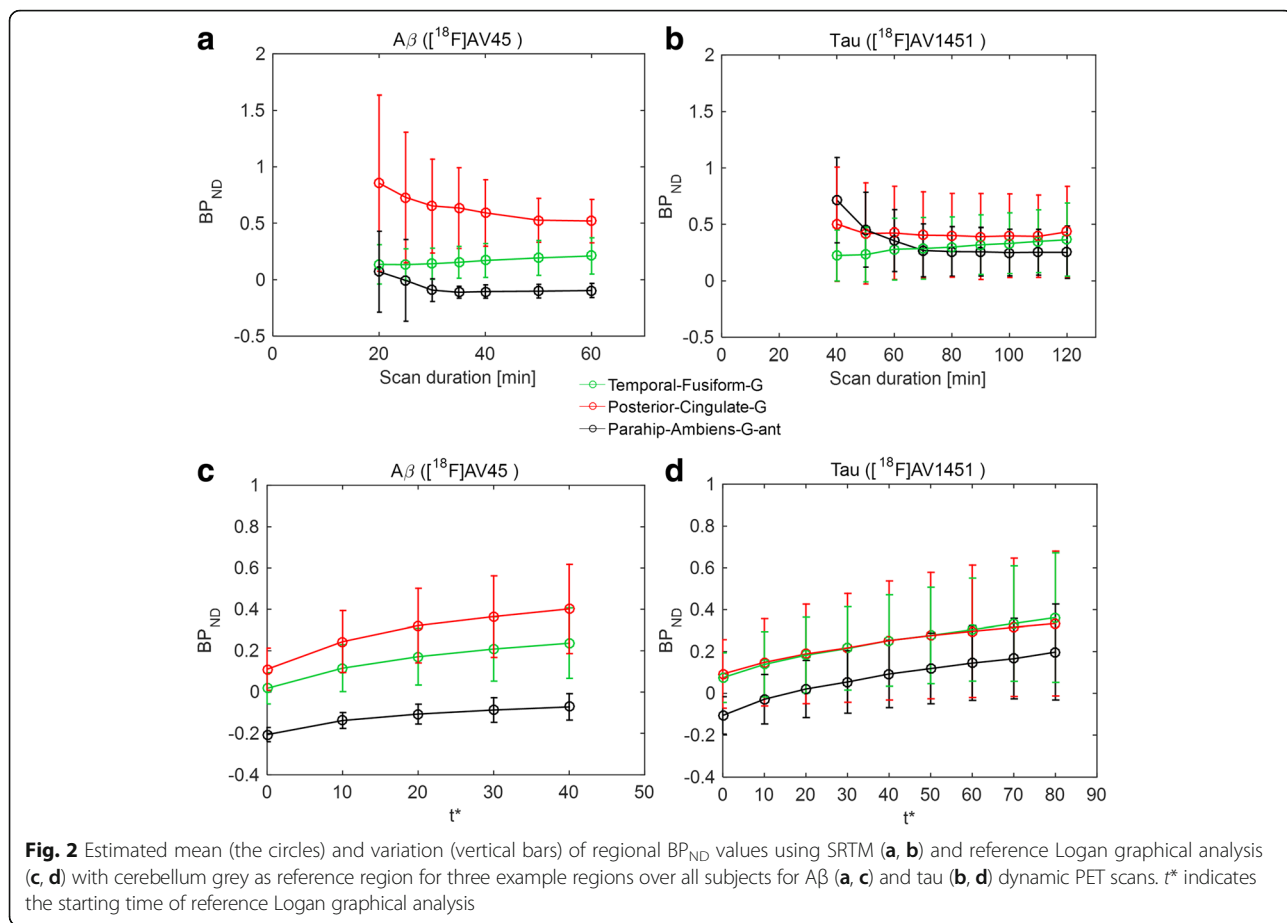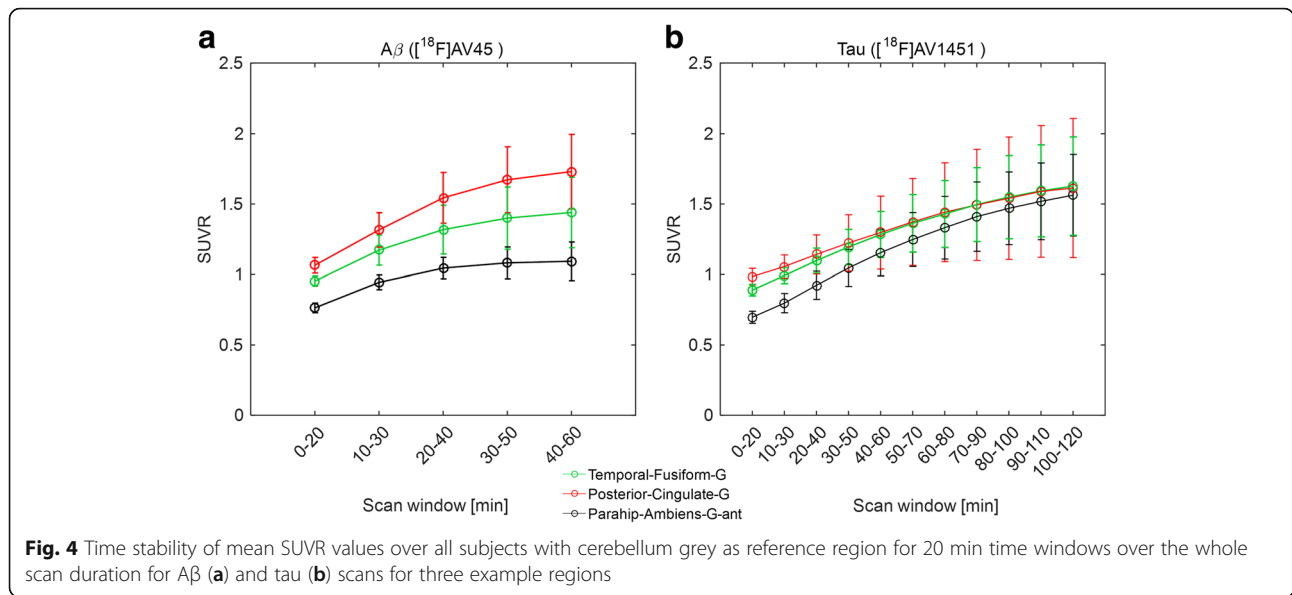

Fig. 1 SRTM (**a**, **b**) and reference Logan graphical analysis model (**c**, **d**) fit (solid line) to TACs (circles) of three example ROIs with different activity levels for Aβ (**a**, **c**; $t^* = 20$) and tau (**b**, **d**; $t^* = 50$) dynamic PET scans

Firouzian *et al. EJNMMI Research* (2018) 8:19

Page 5 of 9

Fig. 2 Estimated mean (the circles) and variation (vertical bars) of regional BP_{ND} values using SRTM (**a**, **b**) and reference Logan graphical analysis (**c**, **d**) with cerebellum grey as reference region for three example regions over all subjects for Aβ (**a**, **c**) and tau (**b**, **d**) dynamic PET scans. *t** indicates the starting time of reference Logan graphical analysis

Fig. 3 Estimated regional BP_{ND} values using SRTM and reference Logan graphical analysis with cerebellum grey as reference region across all subjects for selected regions for Aβ (**a**) and tau (**b**) dynamic PET scans. The BP_{ND} values estimated by reference Logan graphical analysis are for optimum *t** values (*t** = 20 for Aβ and *t** = 50 for tau)

Firouzian *et al. EJNMMI Research* (2018) 8:19

Page 6 of 9

Fig. 4 Time stability of mean SUVR values over all subjects with cerebellum grey as reference region for 20 min time windows over the whole scan duration for Aβ (**a**) and tau (**b**) scans for three example regions

values became stable for scan windows of ∼ 30–50 min p.i. for [^{18}F]AV45 and ∼ 80–100 min p.i. for [^{18}F]AV1451.

To investigate the relationship between the dynamic and static measures, the coefficient of determination (R^2) was calculated for all atlas regions across all subjects between BP_{ND} values, obtained from SRTM and reference Logan graphical analysis methods, and SUVR values of several 20 min time windows. The relationship between these two outcome measures started to stabilize from scan windows of ∼ 40–60 min p.i. for [^{18}F]AV45 and ∼ 80–100 min p.i. for [^{18}F]AV1451. The linear regression analysis of the regional BP_{ND} and SUVR values for the above mentioned time windows showed a high correlation between the two measures using both dynamic methods for both Aβ ($SUVR_{40-60} = 0.97 \times BP_{ND\_SRTM} - 1.2$, $R^2_{SRTM} = 0.75$; $SUVR_{40-60} = 1.11 \times BP_{ND\_Logan} - 1.3$, $R^2_{Logan} = 0.7$; $p < 0.01$) and tau ($SUVR_{80-100} = 1.028 \times BP_{ND\_SRTM} - 1.13$; $R^2_{SRTM} = 0.88$; $SUVR_{80-100} = 1.27 \times BP_{ND\_Logan} - 1.25$; $R^2_{Logan} = 0.71$; $p < 0.01$) PET scans.

Correlation between Aβ and tau tracer signals

The correlation between estimated regional Aβ and tau tracer signals using each of SRTM, reference Logan graphical analysis and SUVR was explored. Twelve different atlas regions with potential of having high Aβ and tau uptake were selected based on the literature and R^2 was calculated for each outcome measure (BP_{ND} or SUVR) for all selected region pairs (Fig. 5). In particular, for the quantitative dynamic analysis methods (SRTM and reference Logan), Aβ signal in the thalamus was highly correlated with tau signal in thalamus ($R^2_{SRTM} = 0.76$, $R^2_{RefLogan} = 0.84$, $p < 0.05$), hippocampus ($R^2_{SRTM} = 0.74$, $R^2_{RefLogan} = 0.73$, $p < 0.05$) and amygdala ($R^2_{SRTM} = 0.56$, $R^2_{RefLogan} = 0.55$, $p < 0.05$). For SUVR, whilst the overall pattern of correlations was
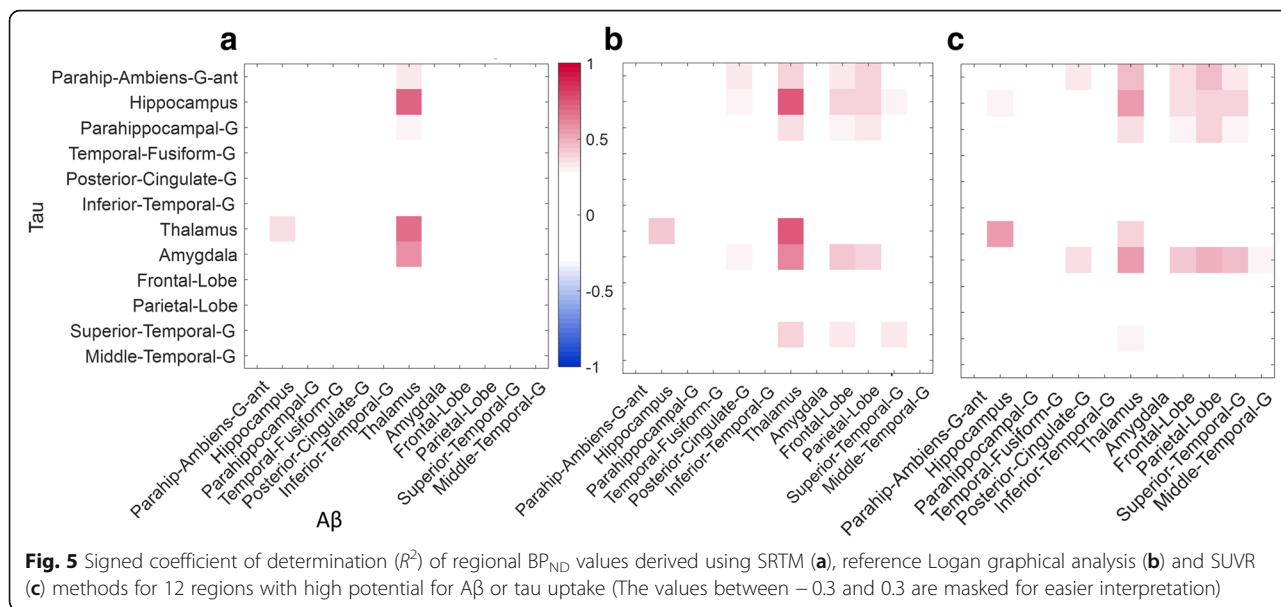
similar, R^2 was reduced (hippocampus: $R^2_{SUVR} = 0.58$, thalamus: $R^2_{SUVR} = 0.46$ and amygdala: $R^2_{SUVR} = 0.57$). The tracer uptake pattern in whole brain, for both [^{18}F]AV45 and [^{18}F]AV1451, are shown in Fig. 6 for all 12 subjects who completed full 60 min of the Aβ PET scan and at least 110 min of the tau PET scan. Overall, the tau signal was very low in all subjects but there was a strong signal observed in the striatal areas. Amyloid signal on the other hand was strong in all brain regions and was not directly related to MMSE scores ($R^2 = 0.006$).

Discussion

In this paper, we assessed the dynamic behaviour of [^{18}F]AV45 and [^{18}F]AV1451 targeting Aβ and tau proteins respectively in early AD subjects by estimating regional BP_{ND} values from dynamic PET scans using SRTM and reference Logan graphical analysis models with cerebellum grey as the reference region.

For the data presented here, arterial input functions were not available and therefore we considered SRTM results from full dynamic data as the reference standard based on previous studies [29, 30]. Comparison of the two dynamic analysis methods (SRTM and reference Logan graphical analysis) showed that they produced similar results with reference Logan graphical analysis slightly underestimating the BP_{ND} values.

Time stability analysis of both tracers demonstrated that stable estimates of the dynamic acquisition outcome parameter BP_{ND} could be obtained with a minimum acquisition time of 30 min for [^{18}F]AV45 and 80 min for [^{18}F]AV1451. Time stability analysis of the SUVR ratio for static acquisition scenarios indicated that the ratio became reasonably constant in scanning windows of 30–50 min p.i. for [^{18}F]AV45 and 80–100 min p.i. for [^{18}F]AV1451 and
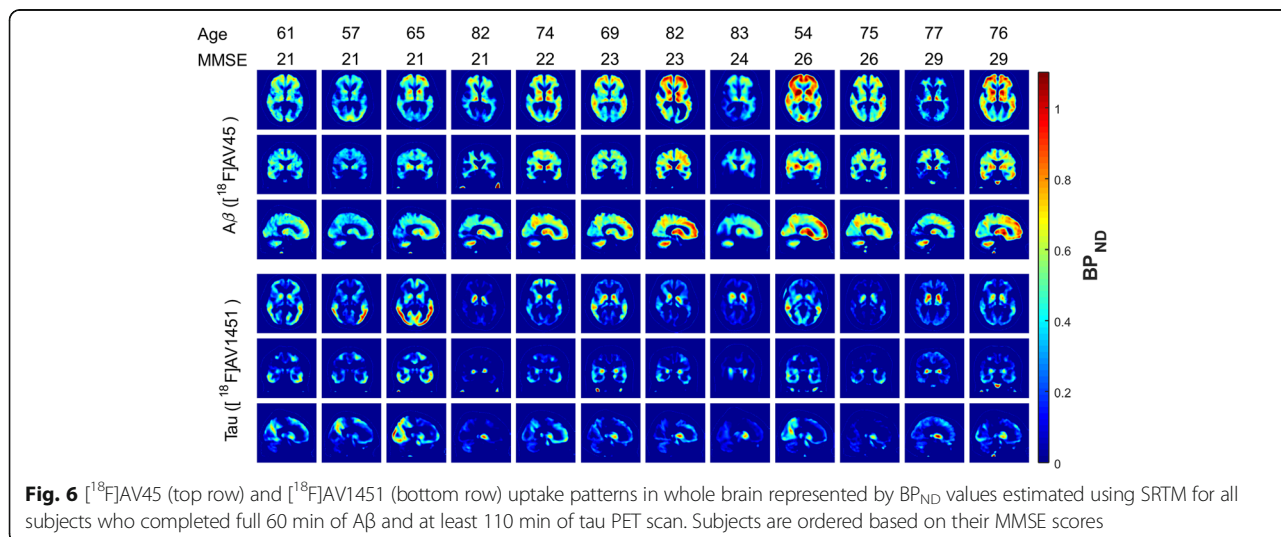
Firouzian *et al. EJNMMI Research* (2018) 8:19

Page 7 of 9

Fig. 5 Signed coefficient of determination (R^2) of regional BP_{ND} values derived using SRTM (**a**), reference Logan graphical analysis (**b**) and SUVR (**c**) methods for 12 regions with high potential for Aβ or tau uptake (The values between − 0.3 and 0.3 are masked for easier interpretation)

were well correlated with the full dynamic SRTM results across regions and subjects ($R^2 = 0.74$ and $R^2 = 0.88$, respectively) [31, 32]. These results are consistent with the faster kinetics of [18F]AV45 as compared to [18F]AV1451.

These results demonstrate that short static acquisitions, whilst reducing subject time in the scanner and improving compliance and feasibility, can derive semi-quantitative outcome measures that can be used for classification of subjects. Their use in longitudinal and intervention studies requires a little more caution as SUVR is not completely independent of blood flow changes [33].

Given the regional binding values for both tracers ([18F]AV45 and [18F]AV1451) in all subjects using SRTM, it was possible to explore the correlations between [18F]AV45 and [18F]AV1451 uptake in different brain regions. In this pilot data set, there was a high

correlation between [18F]AV45 uptake in thalamus and [18F]AV1451 uptake in hippocampus. A degree of caution should be taken in interpreting these results given the low level of amyloid in the thalamus and issues with [18F]AV1451 due to off-target binding and possible spillover from the choroid plexus into the hippocampus. Nevertheless, from a biological stand point, the neuropathology literature [34] shows that dual amyloid and tau changes in the thalamus mirror those in the hippocampus. In addition, the changes in the thalamus affect preferentially those nuclei with hippocampal connections. Therefore, the current results, while speculative and potentially accounted for by off-target binding, suggest that linked thalamus-hippocampus dual pathology reported in neuropathology studies may be demonstrable using PET scans. Thus, it would be important

Fig. 6 [18F]AV45 (top row) and [18F]AV1451 (bottom row) uptake patterns in whole brain represented by BP_{ND} values estimated using SRTM for all subjects who completed full 60 min of Aβ and at least 110 min of tau PET scan. Subjects are ordered based on their MMSE scores

Firouzian *et al. EJNMMI Research* (2018) 8:19

Page 8 of 9

to replicate these results with an improved tau tracer and in a larger cohort of subjects.

Whilst, $[^{18}F]AV45$ and other EMA- and FDA-approved radiotracers have been shown to be highly selective for amyloid, the first generation of tau tracers, including $[^{18}F]AV1451$, have demonstrated some off-target binding. Much of the off-target binding of putative tau agents has focused on monoamine oxidase (MAO) with $[^{18}F]AV1451$ demonstrating some clear subcortical signals due to its binding to MAO-A [35, 36]. Thus, the interpretation of any subcortical $[^{18}F]AV1451$ signal should be treated with a degree of caution. Other first generation tau tracers, such as $[^{18}F]THK5351$ ($[^{18}F]GE216$) [37, 38], have shown even more substantial problems with a large amount of off-target binding to MAO-B that also compromises the interpretation of cortical regions [35]. Second generation tau tracers are now just appearing with $[^{18}F]GTP1$ [39], $[^{18}F]RO6958948$ [40] and $[^{18}F]MK6240$ [41] all demonstrating cleaner signals with increased selectivity for tau.

Conclusions
Based on the data presented, short (20 min) static PET scans at appropriate time windows provide SUVR values which are in reasonable agreement with BP_{ND} values calculated from dynamic scans using SRTM. Appropriate scan window choices for $[^{18}F]AV45$ are 30–50 or 40–60 min p.i., and for $[^{18}F]AV1451$ are 80–100 or 90–110 min p.i. based on the desired accuracy and logistics. Care should be taken to determine whether this outcome measure is optimal in interventional studies.

Abbreviations
AD: Alzheimer's disease; ADAS-Cog: Alzheimer's disease assessment scale-cognitive; Aβ: Amyloid-β; BET: Brain extraction tool; BP_{ND}: Non-displaceable binding potential; CSF: Cerebrospinal fluid; CT: Computed tomography; DPUK: Dementias platform UK; EEG: Electroencephalography; EMA: European medicines agency; FBP: Filtered back projection; FDA: Food and drug agency; FMRIB: Functional MRI of the brain; FSL: FMRIB software library; GCP: Good clinical practice; HIS: Hachinski ischemic score; ICF: Informed consent form; ICH: International conference on harmonisation; MAO: Monoamine oxidase; MEG: Magnetoencephalography; MIAKAT: Molecular imaging and kinetic analysis toolbox; MMSE: Mini mental state examination; MNI: Montreal neurological institute; MRC: Medical research council; MRI: Magnetic resonance imaging; NFT: Neurofibrillary tangles; NIA-AA: National institute of aging-Alzheimer's association; NIHR: National institute for health research; PET: Positron emission tomography; p.i.: post injection; ROI: Region of interest; SPM: Statistical parametric mapping; SRTM: Simplified reference tissue model; SUVR: Standardized uptake value ratio; TAC: Time activity curve

Publisher's Note
Springer Nature remains neutral with regard to jurisdictional claims in published maps and institutional affiliations.

Author details
^{1}Imanova Ltd., Burlington Danes Building, Imperial College London, Hammersmith Hospital, Du Cane Road, London W12 0NN, UK. ^{2}Department of Medicine, Faculty of Medicine, Imperial College London, South Kensington Campus, London SW7 2AZ, UK. ^{3}Department of Psychiatry, University of Oxford, Warneford Hospital, Oxford OX3 7JX, UK. ^{4}Nuffield Department of Clinical Neurosciences, University of Oxford, Oxford OX3 9DU, UK. ^{5}Department of Engineering Science, University of Oxford, Oxford, UK.

References
1. Herrup K. The case for rejecting the amyloid cascade hypothesis. Nat Neurosci. 2015;18:794–9.
2. Vos SJB, Xiong C, Visser PJ, et al. Preclinical Alzheimer's disease and it's outcome: a longitudinal cohort study. Lancet Neurol. 2014;12:957–65.
3. Insel PS, Ossenkoppele R, Gessert D, et al. Time to amyloid positivity and preclinical changes in brain metabolism, atrophy, and cognition: evidence for emerging amyloid pathology in Alzheimer's disease. Front Neurosci. 2017;11:281–9.
4. Bateman R, Xiong C, Benzinger TL, et al. Clinical and biomarker changes in dominantly inherited Alzheimer's disease. N Engl J Med. 2012;367:795–804.
5. Nordberg A. Molecular imaging in Alzheimer's disease: new perspectives on biomarkers for early diagnosis and drug development. Alzheimers Res Ther. 2011;3:34–42.
6. Sevigny J, Chiao P, Bussière T, et al. The antibody aducanumab reduces Aβ plaques in Alzheimer's disease. Nature. 2016;537:50–6.
7. Selkoe DJ, Hardy J. The amyloid hypothesis of Alzheimer's disease at 25 years. EMBO Mol Med. 2016;8:595–608.
8. Klunk WE, Engler H, Nordberg A, etal. Imaging brain amyloid in Alzheimer's disease with Pittsburgh compound-B. Ann Neurol. 2004;55:306–19.
9. Rinne JO, Brooks DJ, Rossor MN, et al. 11C-PiB PET assessment of change in fibrillar amyloid-β load in patients with Alzheimer's disease treated with bapineuzumab: a phase 2, double-blind, placebo-controlled, ascending-dose study. Lancet Neurol. 2010;9:363–72.
10. Okamura N, Harada R, Furumoto S, et al. Tau PET imaging in Alzheimer's disease. Curr Neurol Neurosci Rep. 2014;14:500.

Firouzian *et al. EJNMMI Research* (2018) 8:19

Page 9 of 9

11. Chien DT, Bahri S, Szardenings AK, et al. Early clinical PET imaging results with the novel PHF-Tau radioligand F-18 -T807. J Alzheimers Dis. 2013;34:457–68.

12. Okamura N, Furumoto S, Fodero-Tavoletti MT, et al. Non-invasive assessment of Alzheimer's disease neurofibrillary pathology using 18F-THK5105 PET. Brain. 2014;137:1762–71.

13. Villemagne VL, Furumoto S, Fodero-Tavoletti MT, et al. In vivo evaluation of a novel tau imaging tracer for Alzheimer's disease. Eur J Nucl Med Mol Imaging. 2014;41:816–26.

14. Passamonti L, Vázquez Rodríguez P, Hong YT, et al. 18 F-AV-1451 positron emission tomography in Alzheimer's disease and progressive supranuclear palsy. Brain. 2017;140:781–91.

15. Lammertsma AA, Hume SP. Simplified reference tissue model for PET receptor studies. NeuroImage. 1996;4:153–8.

16. Gunn RN, Lammertsma AA, Hume SP, Cunningham VJ. Parametric imaging of ligand-receptor binding in PET using a simplified reference region model. NeuroImage. 1997;6:279–87.

17. Logan J, Fowler JS, Volkow ND, et al. Distribution volume ratios without blood sampling from graphical analysis of PET data. J Cereb Blood Flow Metab. 1996;16:834–40.

18. Jack CR Jr, Albert M, Knopman DS, et al. Introduction to revised criteria for the diagnosis of Alzheimer's disease: National Institute on Aging and the Alzheimer Association Workgroups. Alzheimers Dement. 2011;7:257–62.

19. McKhann G, Knopman DS, Chertkow H, et al. The diagnosis of dementia due to Alzheimer's disease: recommendations from the National Institute on Aging- Alzheimer's Association workgroups on diagnostic guidelines for Alzheimer's disease. Alzheimers Dement. 2011;7:263–9.

20. Albert MS, DeKosky ST, Dickson D, et al. The diagnosis of mild cognitive impairment due to Alzheimer's disease: recommendations from the National Institute on Aging-Alzheimer's Association workgroups on diagnostic guidelines for Alzheimer's disease. Alzheimers Dement. 2011;7:270–9.

21. Sperling RA, Aisen PS, Beckett LA, et al. Toward defining the preclinical stages of Alzheimer's disease: recommendations from the National Institute on Aging- Alzheimer's Association workgroups on diagnostic guidelines for Alzheimer's disease. Alzheimers Dement. 2011;7:280–92.

22. Koychev I, Gunn RN, Firouzian A, et al. PET tau and amyloid-β burden in mild Alzheimer's disease: divergent relationship with age, cognition, and cerebrospinal fluid biomarkers. J Alzheimers Dis. 2017;60:283–93.

23. Mugler JP, Brookeman JR. Three-dimensional magnetization-prepared rapid gradient-echo imaging (3D MP RAGE). Magn Reson Med. 1990;15:152–7.

24. Jenkinson M, Beckmann CF, Behrens TEJ, Woolrich MW. Smith SM. Fsl Neuroimage. 2012;62:782–90.

25. Smith SM. Fast robust automated brain extraction. Hum Brain Mapp. 2002;17:143–55.

26. William P, Friston K, Ashburner J, Kiebel S, Nichols T. Statistical parametric mapping: the analysis of functional brain images. 1st ed. London: Academic Press; 2007.

27. Grabner G, Janke AL, Budge MM, et al. Symmetric atlasing and model based segmentation: an application to the hippocampus in older adults. In: Med Image Comput Comput Assist Interv; 2006. p. 58–66.

28. Tziortzi AC, Searle GE, Tzimopoulou S, et al. Imaging dopamine receptors in humans with [11C]-(+)-PHNO: dissection of D3 signal and anatomy. NeuroImage. 2011;54:264–77.

29. Wooten D, Guehl NJ, Verwer EE, et al. Pharmacokinetic evaluation of the tau PET radiotracer [18F]T807 ([18F]AV-1451) in human subjects. J Nucl Med. 2017;58:484–91.

30. Hahn A, Schain M, Erlandsson M, et al. Modeling strategies for quantification of in vivo 18 F-AV-1451 binding in patients with tau pathology. J Nucl Med. 2017;58:623–31.

31. Barret O, Alagille D, Sanabria S, et al. Kinetic modeling of the tau PET tracer 18 F-AV-1451 in human healthy volunteers and Alzheimer disease subjects. J Nucl Med. 2017;58:1124–31.

32. Baker SL, Lockhart SN, Price JC, et al. Reference tissue–based kinetic evaluation of ^{18} F-AV-1451 for tau imaging. J Nucl Med. 2017;58:332–8.

33. Cselényi Z, Farde L. Quantification of blood flow-dependent component in estimates of beta-amyloid load obtained using quasi-steady-state standardized uptake value ratio. J Cereb Blood Flow Metab. 2015;35:1485–93.

34. Braak H, Braak E. Neuropathological staging of Alzheimer-related changes. Acta Neuropathol. 1991;82:239–59.

35. Saint-Aubert L, Lemoine L, Chiotis K, et al. Tau PET imaging: present and future directions. Mol Neurodegener. 2017;12:19–40.

36. Sander K, Lashley T, Gami P, et al. Characterization of tau positron emission tomography tracer [18F] AV-1451 binding to postmortem tissue in Alzheimer's disease, primary tauopathies, and other dementias. Alzheimers Dement. 2016;12:1116–24.

37. Lockhart SN, Baker SL, Okamura N, et al. Dynamic PET measures of tau accumulation in cognitively normal older adults and Alzheimer's disease patients measured using [18F] THK-5351. PLoS One. 2016;11:e0158460.

38. Harada R, Okamura N, Furumoto S, et al. 18F-THK5351: a novel PET radiotracer for imaging neurofibrillary pathology in Alzheimer's disease. J Nucl Med. 2015;57:208–14.

39. Jovalekic A, Koglin N, Mueller A, Stephens AW. New protein deposition tracers in the pipeline. EJNMMI Radiopharm Chem. 2016;1:11–22.

40. Wong DF, Kuwabara H, Comley R, et al. Longitudinal changes in [18F]RO6958948 tau PET signal in four Alzheimer's subjects. In: 11th Hum. Amyloid Imaging, Miami, USA, 11 January - 13 January 2017, abstract ID 129, 70.

41. Salinas C, Chiao P, Purohit A, et al. Quantitative analysis and correlation with clinical endpoints of [18F]MK6240 targeting neurofibrillary, tangles (NFTs) in healthy volunteers and subjects with Alzheimer's disease. In: 11th Hum. Amyloid Imaging, Miami, USA, 11 January - 13 January 2017, abstract ID 59, 50.